JOURNAL OF GEOPHYSICAL RESEARCH, VOL. 89, NO. A2, PAGES 925-935, FEBRUARY 1, 1984

Correlation Of Auroral Hiss And Upward Electron Beams Near The Polar Cusp

C. S. LIN AND J. L. BURCH

Department of Space Sciences, Southwest Research Institute

S. D. SHAWHAN AND D. A. GURNETT

Department of Physics and Astronomy, The University of Iowa

Simultaneous plasma and wave data obtained by the DE-1 satellite are used to study a correlation between electrostatic auroral hiss emissions at several kilohertz and upward electron beams at altitudes between 2 and 4 R_E near the dayside polar cusp. Among five randomly selected DE-1 passes, intense electrostatic hiss emissions at frequencies below the electron plasma frequency are found to be associated with strong upward electron beams for every pass. The frequency-time spectrum of auroral hiss near the polar cusp is sometimes characterized by a funnel shape, suggesting that the radiation is emitted from a wave source below the spacecraft. At the center of the enhanced wave region, the electron distribution function above 20 eV is characterized by two components: a hot Maxwellian component and an upward electron beam. The beams generally have a peak energy around 50 eV, a temperature around 20 eV and a density of the order of 1 cm^{-3}. The observed distribution functions are fitted by a drifting Maxwellian function for the electron beam and an isotropic Maxwellian function for the hot component. The empirically fitted plasma parameters are then used to solve the linear dispersion equation of electrostatic waves. The instability analyses indicate that whistler waves propagating with wave normal angles near a small resonance cone can be easily excited by low energy (<100 eV) upward electron beams. The frequencies of large growth rates are found below the electron plasma frequency, in agreement with the observations. On the basis of the model that cusp auroral hiss emissions are whistler waves propagating near the resonance cone, ray path studies indicate that the low altitude boundary of the wave source of cusp hiss is located at about 1 R_E.

INTRODUCTION

The DE-1 satellite has made in situ plasma and field measurements across the polar cusp at radial distances between 2 and 5 R_E. Many new interesting results have already been reported (e.g. see *Geophysical Research Letters*, September 1982). Of particular interest to this article is the observation of upward electron beams at energies below 100 eV equatorward of and within the polar cusp [*Burch et al.*, 1983]. Simultaneous magnetic field measurements on DE-1 showed a reversal of the east-west magnetic-field component, indicating downward field-aligned currents in the region of the electron beams. These upward electron beams were thus believed to be charge carriers of the dayside region 1 field-aligned currents. In this article, we report a correlation of intense electrostatic waves at several kilohertz (kHz) with these upward electron beams. Such a correlation has not been reported previously for lack of observations at high altitudes within the dayside cusp.

The electrostatic hiss emissions studied here are very similar to the auroral hiss observed by the DE-1 satellite in the nightside auroral zone [*Gurnett et al.*, 1983]. The nightside auroral hiss observed at the DE-1 altitude was mainly electrostatic and was believed to be whistler waves propagating upward at wave normal angles near the resonance cone from a wave source that has a lower boundary located between 0.7 and 0.9 R_E altitude. At lower altitudes (<3000 km) the auroral hiss is electromagnetic and frequently detected by satellites as downward propagating whistler waves [*Gurnett and Frank*, 1972; *Shawhan*, 1979]. The auroral hiss emission at lower altitudes has been found to be closely correlated with intense fluxes of low energy, 100 eV to 1 keV, precipitating electrons in the dayside auroral zone [*Gurnett*, 1966; *Hoffman and Laaspere*, 1972]. In the nightside auroral zone, *Gurnett and Frank* [1972] specifically showed that an auroral hiss event occurred in direct association with an intense inverted V electron precipitation event. It is well known that intense electron inverted V electron fluxes are characterized by downward beams with a beam energy typically about several keV [*Lin and Hoffman*, 1982]. As will be reported in this article, the electron beams correlated with the dayside cusp hiss emission are not related to inverted V events because these beams are moving in the upward direction.

Simultaneous measurements of wave spectra and electron distribution functions by the DE-1 satellite have made possible detailed comparative studies of observations and wave instability theory. Previously, various theoretical investigations have shown that auroral electron beams with peak energies of several keV can excite whistler waves with a propagation angle near the resonance cone via the Landau resonance [*Swift and Kan*, 1975; *James*, 1976; *Maggs*, 1976, 1978]. This wave excitation mechanism, sometimes known as Cherenkov amplification, appears to explain the observed intensities of auroral hiss that propagates downward at low altitudes (<1 R_E). It has been suggested that the VLF saucers [*Gurnett and Frank*, 1972; *James*, 1976] and the upward propagating auroral hiss [*Gurnett et al.*, 1983] can be excited by upward moving low energy (<100 eV) electrons, although the existence of such low energy electron beams reported by *Burch et al.* [1983] was not known at that time. The present study will use the observed electron distribution functions to conduct an instability analysis and demonstrate that the upward electron beams observed near the cusp could excite the cusp auroral hiss.

In this article we present data obtained from the DE-1 high-

Copyright 1984 by the American Geophysical Union.

Paper number 3A1549
0148-0227/84/003A-1549$05.00

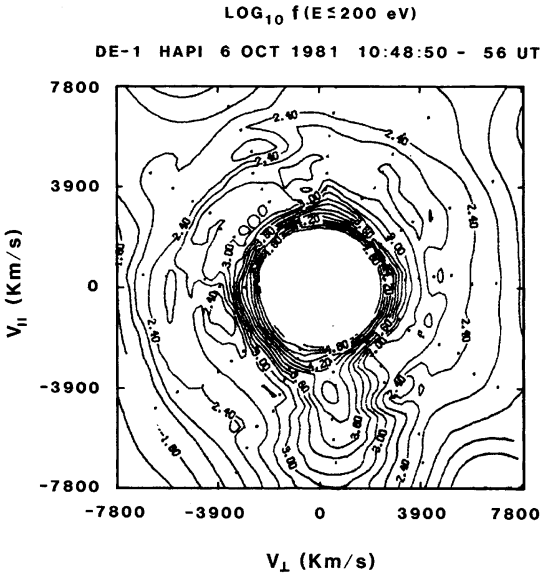

Fig. 1. Phase-space density contours of the logarithm of the electron distribution function. The contours are labeled every 0.6 units from 1.80 to 4.80. The dots are loci of the data used for contouring. An upward electron beam is displayed as a contour island centered on the negative $V_{||}$ axis.

altitude plasma instrument (HAPI) and plasma wave instrument (PWI) during outbound passes through the polar cusp near local noon. We fit the observed distribution functions of electron beams by drifting Maxwellian functions and the observed distribution functions of hot background electrons by isotropic Maxwellian functions. In addition, the cold plasma density is inferred from knowledge of the electron plasma frequency and the measured density of the warm plasma, including the electron beam distribution. The empirically fitted plasma parameters, including density, temperature, and drifting energy, are used to solve the linear dispersion equation for the resulting whistler mode emissions. Because the whistler mode becomes quasi-electrostatic for wave-normal angles near the resonance cone, the electrostatic approximation is used for the whistler mode dispersion relation. The results of wave instability analyses are then compared with the wave observations. A ray tracing of cusp hiss emission is conducted to locate the wave source region.

INSTRUMENTATION

The HAPI instrument consists of five identical electrostatic analyzers at separate viewing angles, each making simultaneous measurements of electrons and ions at up to 64 energy steps from 5 eV to 31 keV. For the events of interest, HAPI was operated at 30 energy steps every 1/2 s and measured the complete distribution function in every spin period (≈6 s). The detector viewing angles are respectively 45°, 78°, 90°, 102°, and 135° relative to the spacecraft spin axis, which is oriented perpendicular to the orbital plane. A detailed description of the HAPI experiment is given in the work of *Burch et al.* [1981].

The plasma wave instrument uses two electric dipole antennas for electric field measurements: one with a length of 9 m tip to tip oriented parallel to the spin axis and the other with a length of 215 m tip to tip oriented perpendicular to the spin axis. A magnetic loop antenna is also available to distinguish between electrostatic and electromagnetic waves. A detailed description of the plasma wave instrumentation is given by *Shawhan et al.* [1981]. For a description of the DE-1 spacecraft, see *Hoffman and Schmerling* [1981].

OBSERVATIONS

The DE-1 satellite frequently observed the correlation of hiss emissions and electron beams near the dayside polar cusp. Among five randomly selected DE-1 passes through the polar cusp, intense upward electron beams were found equatorward of and within the cusp for every pass. Furthermore, the electron beams were found to be associated with the enhancement of hiss emissions at a few kilohertz. To illustrate the wave-beam correlation observed by DE-1, we discuss two representative passes through the dayside cusp. These two passes were at magnetic local times (MLT) near local noon and at altitudes between 2.5 and 3.5 R_E. The particle energy-time spectrograms for these passes are shown in Plates 1 and 2, and the corresponding wave frequency-time spectrograms are shown in Plates 3 and 4. Additional examples of particle spectrograms for dayside cusp crossings can be found in the paper by *Burch et al.* [1983].

Day 279, 1981

The first representative pass, in Plate 1, is an outbound pass near local noon at a magnetic local time of about 11.5 hours. The DE-1 spacecraft approached the dayside cusp at an altitude of about 21,000 km and an invariant latitude of about 79°. The top energy-time spectrogram, where electron differential energy fluxes are color-coded, illustrates typical features observed by DE-1 equatorward of the dayside cusp. The satellite, moving poleward, detected first a region of uniform fluxes of trapped energetic electrons (>1 keV) until 1047 UT. From 1047 to 1049:20 UT, DE-1 passed through a transition region where much weaker fluxes of trapped energetic electrons and intense low energy (<500 eV) cusp electron fluxes were detected simultaneously. The lower spectrogram shows that weak ion fluxes with energy between 100 and 1000 eV were also present in this region. These ion fluxes have been identified as conic ions [*Sharp et al.*, 1977]. Intense electron beams at energies below 100 eV can be easily identified as bright-color vertical stripes in the top spectrogram from 1048:20 to 1049:10 UT. These beams were moving upward because their pitch angles shown in the middle panel were near 180°. Downward electron beams were also present during this interval but were too weak to be recognized from the spectrogram. The DE-1 satellite finally moved into the polar cusp at about 1049:20 UT, detecting a significant intensification of low-energy electron fluxes and the first appearance of cusp ion fluxes. Inside the cusp, the ion fluxes gradually developed a V shaped energy/pitch angle distribution as described by *Burch et al.* [1982].

The distribution function f of the low energy cusp electrons with an upward electron beam is illustrated in a contour plot of log f for a 6-s time interval (Figure 1). An electron beam with a beam velocity of about -3900 km/s can be clearly identified along the $-V_{||}$ axis. Particle velocity in the upward direction is defined as negative in the northern hemisphere. From the contour spacings, the temperature of the electron

beam appears to be greater in the parallel direction than in the perpendicular direction. Figure 1 indicates that low-energy cusp electrons have a hot isotropic component in addition to the beam component. The contour plot contains a hole in the center because only measurements at energies greater than 20 eV were used. Electron data below 20 eV were dominated by spacecraft photoelectrons and thus are excluded in this study.

To illustrate the intensity of these electron beams, we present line plots of distribution functions with pitch angles near 180° (Figure 2). This figure shows the distribution functions measured simultaneously during one energy sweep. The distribution function with pitch angles between 170° and 177° (solid line) has a significant peak near 50 *eV*, while the distribution function at slightly lower pitch angles (160°—170°) has no peak (dashed line). The peak value of the distribution function of this electron beam is about 10^4 s^3/km^6, about an order of magnitude greater than the distribution function of the isotropic component at the corresponding energy. We estimate that the half angular width of the electron beam was only about 10°. The distribution function with pitch angles less than 170° is representative for the isotropic component of low energy cusp electrons shown in Figure 1. This component can be approximated by a Maxwellian function since log f decreases linearly with energy. The detailed analysis of this method of characterizing the isotropic component and the electron beam is described in the data analysis section.

The plasma wave measurements of electric field intensity for this polar cusp crossing are shown in Plate 3. This frequency-time spectrogram displays intense wave emissions at a few kilohertz with the shape of half a "funnel" from 1010 to 1050 UT. The upper cutoff frequency of this funnel-shaped emission is near 10 kHz, and the lower freuency cutoff decreases gradually from near 10 kHz to several hundred hertz. The "funnel" shape is a propagation effect that occurs for whistler mode waves propagating upward from a source below the satellite (e.g., see Gurnett et al. [1983]). The funnel is caused by the frequency dependence of the ray path when the wave normal angle is near the resonance cone, where the whistler mode is electrostatic. Separate wave magnetic field measurements (not shown) indicate that correlated magnetic wave fields were absent before 1048 UT and weak afterward, thereby confirming the electrostatic character of the wave. The whistler mode has an upper cutoff frequency slightly below the electron gyrofrequency f_{ce} or the electron plasma frequency f_{pe}, whichever is smaller. After about 1110 UT, the upper cutoff frequency is below the electron plasma frequency since the cutoff is well below the electron gyrofrequency, which is computed according to the MAGSAT II model of magnetic field and indicated by the solid line in the figure.

Plate 3 shows that the cusp hiss emission was intensified about 1048 UT, roughly the same time when the intense upward electron beams were detected. In Figure 3 we present the electric field spectral density (V^2/m^2 Hz) of cusp hiss for a 32-s time interval starting at 1048:43 UT. This figure shows that the spectrum of cusp hiss has a sharp cutoff f_2 at about 13 kHz. This spectrum indicates that f_{pe} was slightly greater than 13 kHz.

Further details of the cusp hiss emission for this event are illustrated in a high resolution wideband spectrogram from 1046 to 1050 UT (Figure 4). The electric field intensity at frequencies up to 40 kHz is presented. This high resolution spectrogram illustrates that the cusp hiss in association with electron beams was detected in bursts (1047—1049:20 UT).

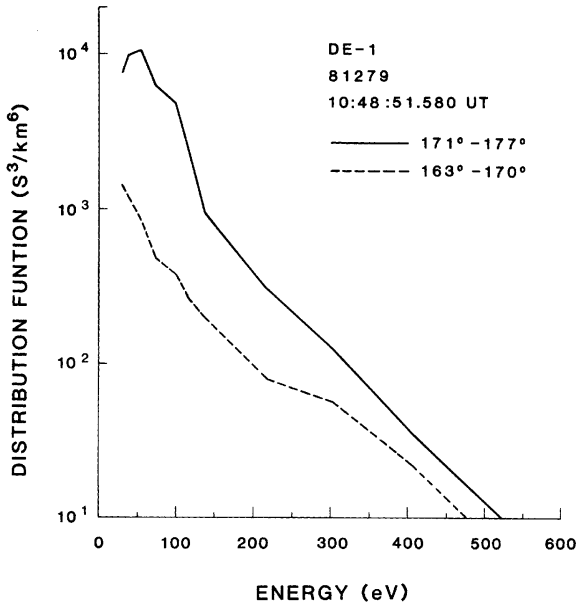

Fig. 2. Electron distribution functions at two pitch angles measured simultaneously.

The upper cutoff frequency fluctuated around 10 kHz, suggesting a fluctuating plasma density in this region. The wave characteristics before and after this time interval were more steady and broadbanded than they were within it. Figure 4 shows that the hiss emission near 1050 UT had an upper cutoff about 12.5 kHz. The hiss emission after 1049:20 UT appears to be similar to the nightside auroral hiss illustrated in Figure 8 of *Gurnett et al.* [1983]. The narrowband emissions at about 20 kHz may be Bernstein waves which can occur at frequencies between f_{ce} and 2 f_{ce}, depending on the hot to cold density ratio. As noted by *Gurnett et al.* [1983], electron cyclotron waves of this type are frequently observed near the cusp.

Day 280, 1981

The second representative pass, in Plate 2, occurred on the next day following the example in Plate 1 at about 17,700 km altitude, 1000 h MLT and 75° invariant latitude. The plasma instrument detected trapped energetic electrons until 1336 UT and low-energy cusp electrons for the next minute. The low energy cusp electron fluxes dropped sharply at energies above 400 eV and contained upward electron beams (bright vertical stripes in the figure near 180° pitch angle). Like the example in Plate 1, the beam energies were around 50 eV. The fine features of the spectrogram indicate that weak downward electron beams were also present at energies comparable to those of the upward electron beams.

One interesting observation of this pass, not seen in the first representative pass (day 81279), is the reappearance of trapped energetic electron fluxes at about 1337 UT for about 1 min. Another short burst of trapped energetic electron fluxes was detected in the midst of cusp electron fluxes at about 1336:10 UT. The DE-1 satellite finally passed through the polar cusp at about 1342 UT, detecting the typical signatures of cusp ion fluxes and intense low energy electron fluxes (not shown). The return of trapped energetic electrons at the DE-1 position before the final encounter of the polar cusp suggests that the polar cusp underwent oscillatory motion, first moving pole-

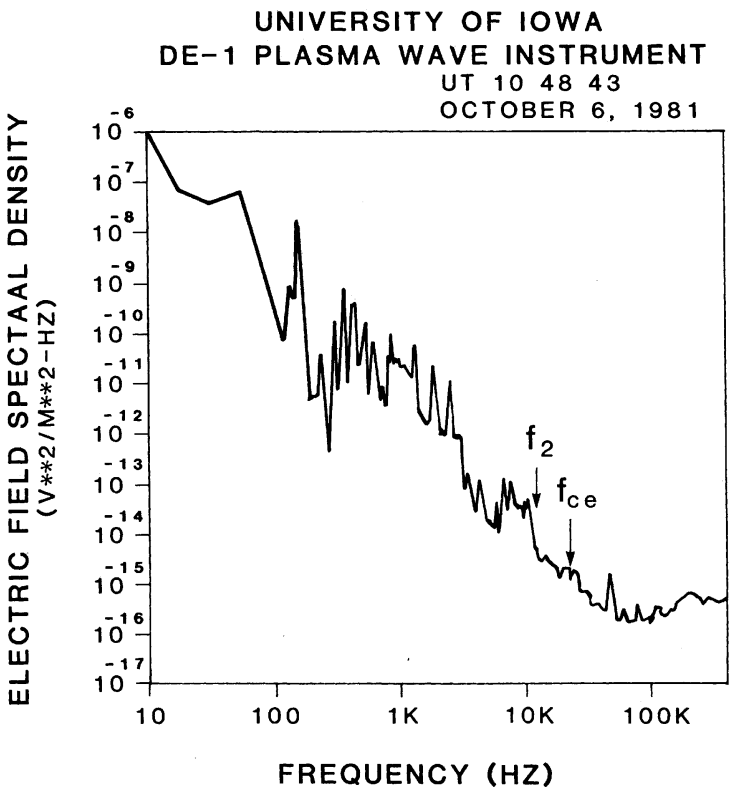

Fig. 3. Electric field spectral density for a 32-s time interval.

ward and then equatorward. Although the dayside cusp is known to move in response to the interplanetary magnetic field and the ring current [*Burch*, 1979; *Meng*, 1983], we are not aware of any previous report on the direct observation of the oscillatory motion of the dayside cusp.

From a single satellite observation, we could not determine the velocity of the cusp boundary motion. But the poleward velocity of the cusp had to be greater than the satellite velocity, which was about 2.8 km/s in the direction perpendicular to the radius vector. If the trapped particle boundary started to move poleward when DE-1 was halfway from the first to the second trapped boundary, then the trapped particle boundary velocity would be about 5.6 km/s. When mapped along a dipole field line, this velocity corresponds to 80 km/s at the equator, which would be in agreement with magnetopause velocities determined from ISEE data [*Parks et al.*, 1978; *Berchem and Russell*, 1982].

The frequency time spectrogram of electric field intensity for this pass shows the enhancement of kilohertz cusp hiss from 1336 UT to 1342 UT (Plate 4). The duration of hiss enhancement covers the period of detecting upward electron beams (1336—1337 UT) (Plate 2). Before 1336 UT, the cusp hiss intensity was weak. The upper cutoff frequency of the cusp hiss was about 20 kHz, while the electron cyclotron frequency shown in the solid line was about 30 kHz around 1336 UT.

DATA ANALYSIS

In this section we present an analysis of plasma data that characterizes the number densities, temperatures, and drifting energies of the measured distribution functions. A nonlinear least square fit was made to the complete distribution function measured during one spin period (≈6 s) for energies between 20 and 400 eV using a double Maxwellian function of the form $f = f_h + f_b$, where

$$f_h = n_h \left(\frac{m}{2\pi T_h}\right)^{3/2} \exp\left(-\frac{mV^2}{2T_h}\right) \quad (1)$$

$$f_b = n_b \left(\frac{m}{2\pi T_b}\right)^{3/2} \exp\{-m[(V_{||} - V_b)^2 + V_\perp^2]/2T_b\} \quad (2)$$

where

- m electron mass;
- n_h number density of the hot component;
- T_h temperature of the hot component;
- n_b number density of the electron beam;
- T_b temperature of the electron beam;
- V_b beam velocity.

Equations (1) and (2) are used because they characterize the basic features of the observed distribution functions (see Figure 2). Furthermore, they are convenient for instability analyses. We used the data at $165° < \alpha < 180°$ to approximate f_b in the upward direction, the data at $\alpha < 15°$ to approximate f_b in the downward direction, and the data at $15° < \alpha < 165°$ to approximate f_h. The temperature anisotropy of electron beams is neglected in this analysis.

The electron beam parameters determined for day 81279 are

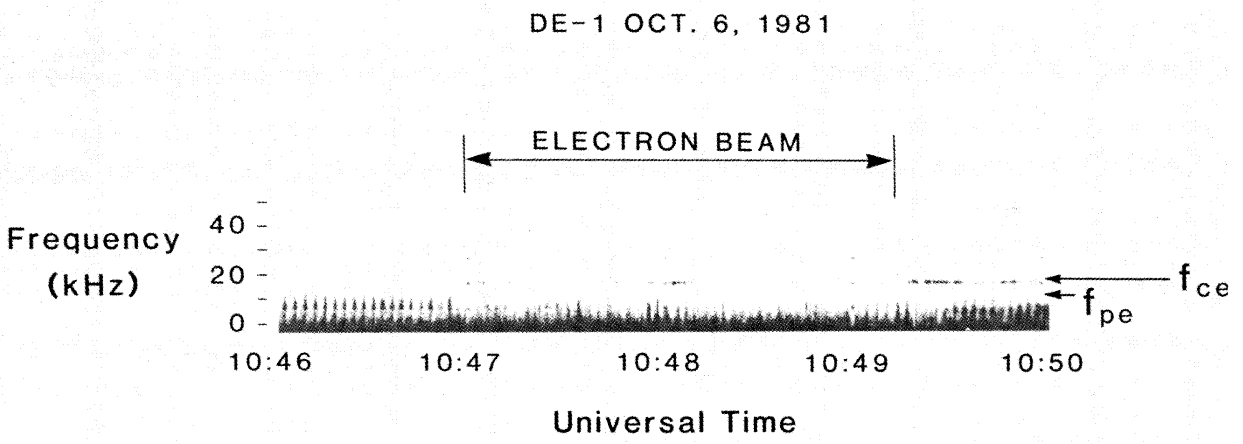

Fig. 4. High resolution frequency-time spectrogram during the detection of an intense upward electron beam on October 6, 1981 (day 279). The electron plasma frequency is marked at a frequency slightly above the upper cutoff on the right hand side of the spectrogram.

shown in Figure 5, where upward electron beams are displayed in open circles and downward electron beams in solid circles. This figure illustrates that the beam energy centered around 50 eV and the temperature varied around 20 eV. The number density of the upward electron beams was very high between 1048:30 and 1049:20 UT, reaching 2 cm^{-3}. The number density of the downward electron beams was generally smaller by an order of magnitude (≤ 0.1 cm^{-3}).

The 6-s averaged number densities and temperatures of the hot component remained fairly constant in the time interval 1047—1049:20 UT. The number density varied within 10% of 1 cm^{-3}. The temperature of the isotropic component was about 100 eV during the minute beginning at 1047 UT, and decreased to about 90 eV in the next minute.

The fitted plasma parameters of the electron beams for the pass of day 81280 illustrated in Figure 2 are similar to the pass of day 81279. The electron beam energy varied around 40 eV. The average temperature of the electron beam was about 20 eV, again less than the beam energy. The beam number densities were clustered around 0.3 cm^{-3} with the exception of one upward beam that had a density of 2 cm^{-3} (around 1336:30 UT). During this pass, the downward electron beams often had a number density comparable to those of upward beams. On the average, the density and temperature of the hot component were about 2 cm^{-3} and 60 eV, respectively.

INSTABILITY ANALYSIS

In this section we describe an instability analysis by using the fitted distribution function presented in the previous section. As an initial study, we concentrate only on the instability of electrostatic waves at frequencies ω below the electron plasma frequency ω_{pe} due to upward electron beams. This study considers only the case $\omega_{pe} < \omega_{ce}$, since the DE-1 plasma and wave measurements suggest $\omega_{pe} < \omega_{ce}$ in the region of electron beams. For $\omega_{pe} < \omega_{ce}$, whistler waves with wave normal angles near the resonance cone Θ become electrostatic. The resonance wave frequency ranges from the lower hybrid resonance frequency at $\Theta = \pi/2$ to ω_{pe} at $\Theta = 0$ [*Shafranov*, 1967]. As Θ approaches zero, the whistler wave mode at the resonance cone merges into the electron plasma wave. The purpose of the following analysis is to demonstrate that these waves can be easily excited by the observed upward electron beams.

The distribution function is assumed to consist of three components: an electron beam, a cold component, and a hot component. We represent the hot component by an isotropic Maxwellian function (equation (1)) and the electron beam by a drifting Maxwellian function (equation (2)). We consider electrostatic waves with an arbitrary propagation angle Θ with respect to the magnetic field direction. For the distribution functions given in equation (1), the linear dispersion equation [*Mikhailovskii*, 1974; *Hasegawa*, 1975] is given by

$$1 + D_c + D_h + D_b = 0 \tag{3}$$

$$D_c = -\frac{\omega_{pi}^2}{\omega^2} - q\frac{\omega_{pe}^2 \cos^2\Theta}{\omega^2} - \frac{q\,\omega_{pe}^2 \sin^2\Theta}{\omega^2 - \omega_{ce}^2}$$

$$D_h = (1-q)(1-r)\frac{2\omega_{pe}^2}{k^2 a_h^2} \cdot \left[1 + \frac{\omega}{k_{||} a_h}\sum_n I_n e^{-\lambda_h} Z\left(\frac{\omega - n\omega_{ce}}{k_{||} a_h}\right)\right]$$

$$D_b = (1-q)\,r\,\frac{2\omega_{pe}^2}{k^2 a_b^2} \cdot \left[1 + \frac{\omega - k_{||} V_b}{k_{||} a_b}\sum_n I_n e^{-\lambda_h} Z\left(\frac{\omega - k_{||} V_b - n\omega_{ce}}{k_{||} a_b}\right)\right]$$

where

$q = n_c/(n_c + n_h + n_b)$;
$r = n_b/(n_h + n_b)$;
$a_j = (2T_j/m)^{1/2}$, where j is a subscript, b or h;
$\lambda_j = (k_\perp^2 a_j^2/2\omega_{ce}^2)$;
$k = (k_{||}^2 + k_\perp^2)^{1/2}$;

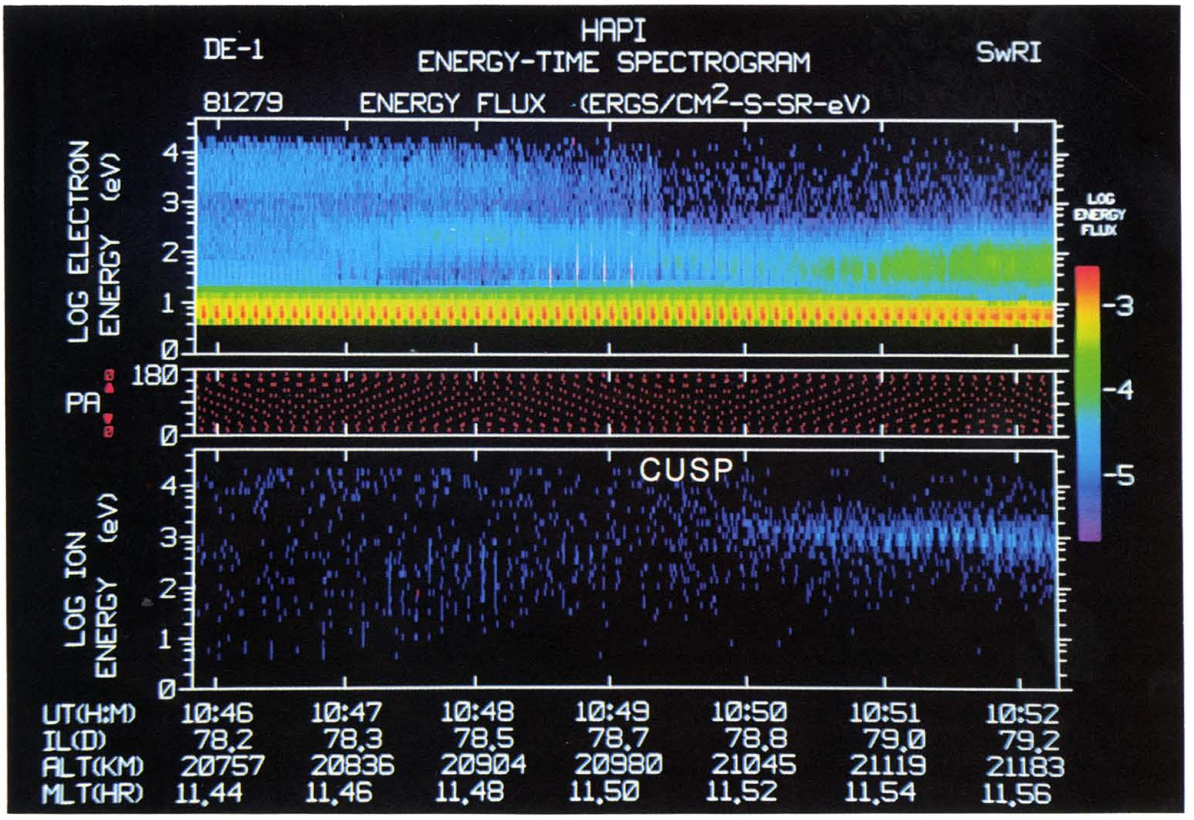

Plate 1. Energy-time spectrograms of electron (top) and ion (bottom) energy fluxes on October 6, 1981. The detector's pitch angle is plotted in the center panel. The satellite coordinate including invariant latitude (IL), altitude (ALT) and magnetic local time (MLT) is given at the bottom.

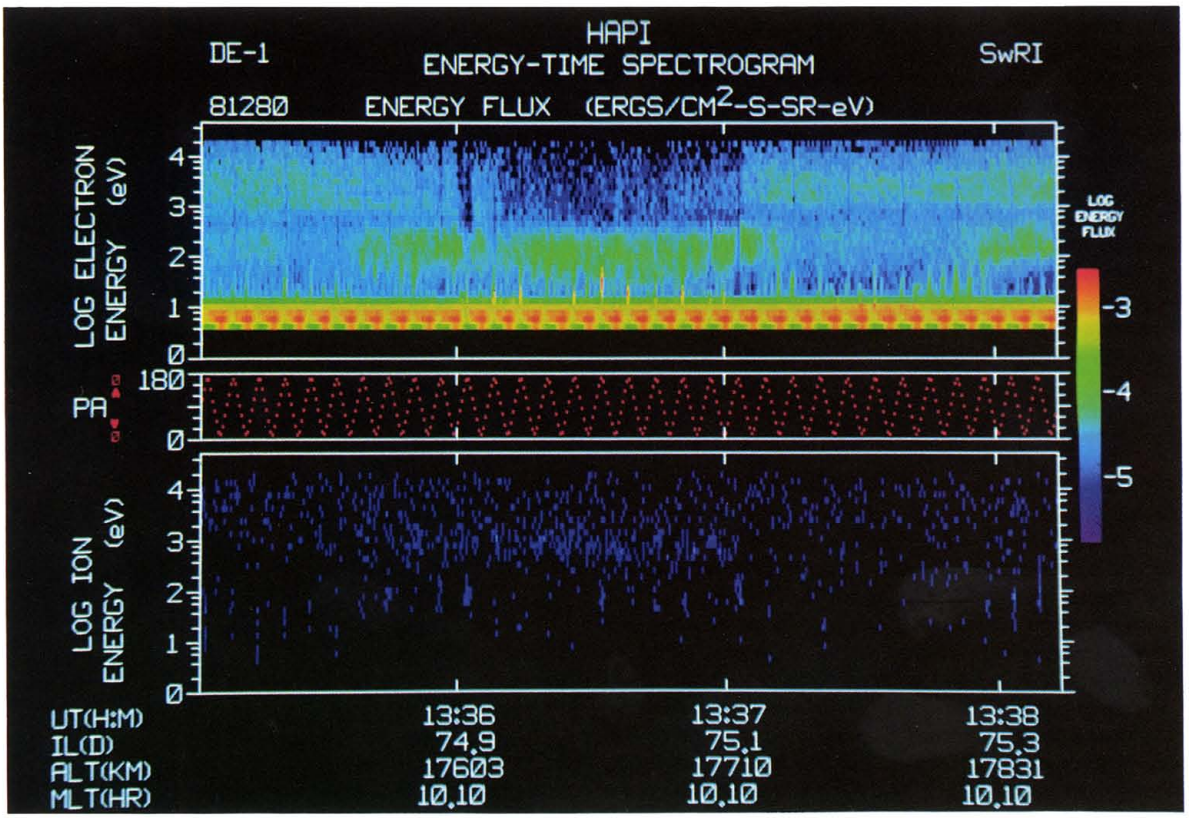

Plate 2. Energy-time spectrogram for electrons and ions on October 7, 1981.

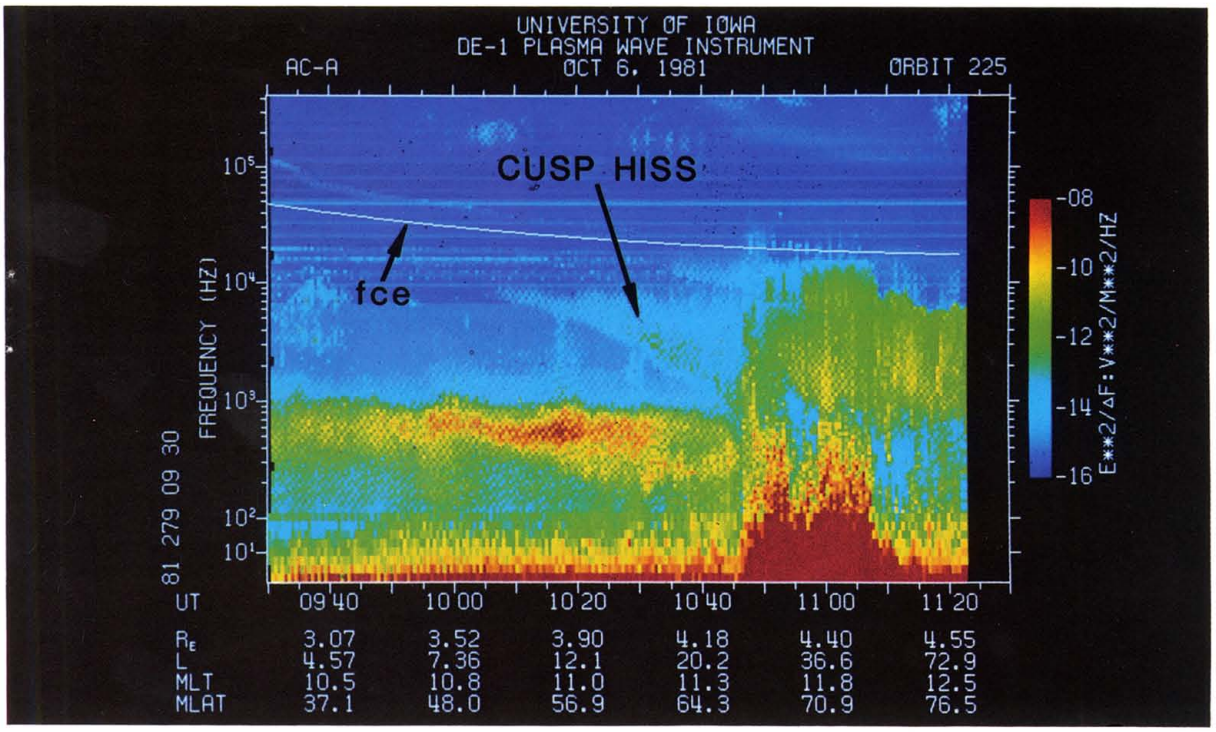

Plate 3. Frequency-time spectrogram of the electric field intensities for a crossing of the dayside polar cusp on October 6, 1981. The electron gyrofrequency, which is larger than the electron plasma frequency in this case, is plotted in solid line.

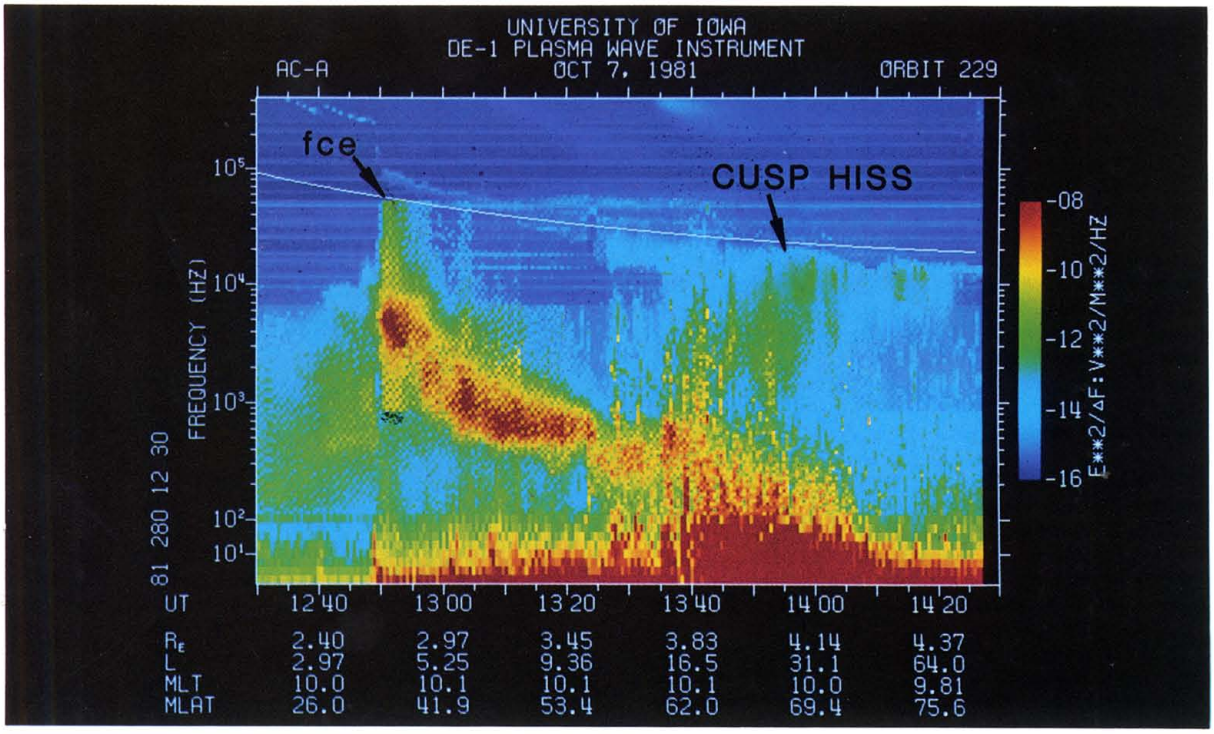

Plate 4. Frequency-time spectrogram on October 7, 1981.

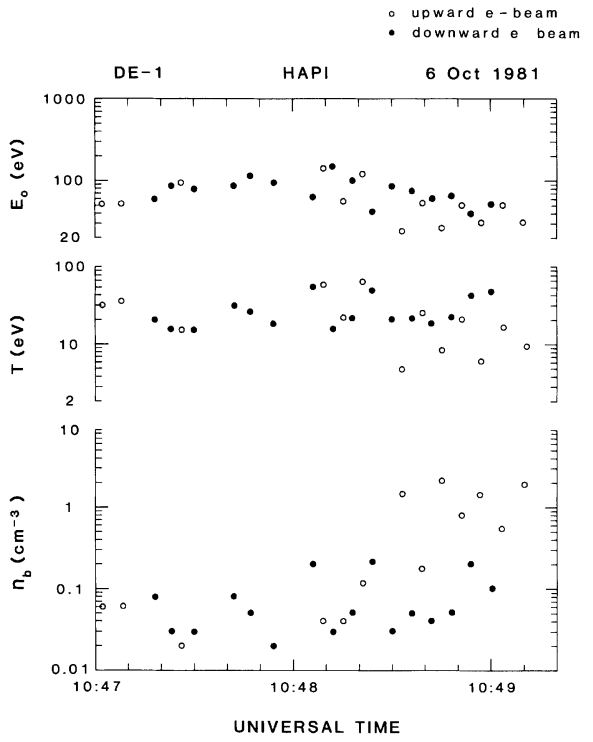

Fig. 5. Fitted parameters of electron beams with number density greater than 0.01 cm^{-3}.

$k_{||}$ component of wave vector parallel to magnetic field;
$k_\perp$ component of wave vector perpendicular to magnetic field;
$I_n(\lambda_i)$ modified Bessel function of order n with argument λ_i;
Z plasma dispersion function.

In solving the dispersion equation, we use the fitted parameters of an intense upward beam illustrated in Figure 5 as an example. The plasma parameters used are $n_b = 0.85$ cm^{-3}, $E_b = 50$ eV, $T_b = 20$ eV, $n_h = 1.05$ cm^{-3}, and $T_h = 86$ eV. These parameters approximately model the observed distribution function in the interval 1048:50 to 1049 UT on day 81279. The wave measurement suggested that f_{pe} was slightly greater than 13 kHz. Therefore, an electron plasma frequency $f_{pe} = 14$ kHz, corresponding to a total plasma density of 2.4 cm^{-3}, is used in the calculation. We thus infer the density of the cold component to be 0.5 cm^{-3}. Using these parameters, we deduce that $q = 0.22$, $r = 0.44$, $T_h/T_b = 4.3$, and $V_b/a_b = 1.6$. The ratio of plasma frequency to the electron gyrofrequency ω_{pe}/ω_{ce} is 0.7 since $f_{ce} = 20$ kHz as shown in Plate 3.

For the parameters given in the preceding paragraph, the dispersion relation of (3) describes interactions of a warm electron beam with a hot and a cold plasma. Beam-plasma instability for such a three component plasma has not been examined previously. Because V_b/a_b and V_b/a_h are near 1, it becomes necessary to solve the dispersion equation in its entirety. Since we are only interested in $\omega < \omega_{pe}$, we keep in (3) terms for harmonics $n = 0, \pm1, \pm2, \pm3$. Therefore, besides Landau resonance ($\omega - k_{||} V_{||} = 0$), the normal cyclotron resonance ($\omega - k_{||} V_{||} - \omega_{ce} = 0$) and anomalous cyclotron resonance ($\omega - k_{||} V_{||} + \omega_{ce} = 0$) are included in the analysis. The results are shown in Figures 6, 7, and 8.

For the modeled distribution function, Figure 6 shows that wave instabiity occurs at normalized frequency $\omega/\omega_{ce} \leqslant 0.32$. Since $\omega_{ce} \approx 20$ kHz, the unstable wave frequency would be less than 6.4 kHz. The frequency range of unstable waves is consistent with the DE-1 observation. The upper frequency cutoff appears to depend on the cold plasma density n_c. To investigate the effects of cold plasma on the instability, we calculate growth rates as a function of n_c, while keeping n_h, n_b, *and* ka_b/ω_{ce} constant. The results obtained for $\Theta = 0°$ are shown in Figure 7. This figure indicates that ω/ω_{ce} and γ/ω_{ce} increase with n_c. In the absence of cold plasma, the wave frequency approaches the ion plasma frequency and the growth rate becomes very small ($\gamma/\omega_{ce} < 10^{-3}$). A small amount of cold plasma is thus needed to explain the observed wave frequency of cusp hiss emission. The observation of the upper cutoff frequency in the range of 4-10 kHz would require n_c to be in the range of 0.2 to 1.4 cm^{-3}. This range of n_c is consistent with the cold plasma density deduced from the wave and plasma data. This result also suggests that the observed fluctuation of the upper cutoff frequency might be caused by a fluctuating n_c.

At constant Θ, the wave frequency increases linearly with ka_b/ω_{ce} for $ka_b/\omega_{ce} \leqslant 0.8$ and remains constant for larger ka_b/ω_{ce} (Figure 6) . The instability growth rate is large, reaching 0.06 at $ka_b/\omega_{ce} \cong 0.4$. The growth rate γ/ω_{ce} is largest when $\Theta = 0°$ and decreases with Θ. Similarly, ω/ω_{ce} decreases from 0.32 at $\Theta = 0°$ to about 0.05 at $\Theta = 80°$. The dependence of ω/ω_{ce} and γ/ω_{ce} on Θ is also illustrated in Figure 8, in which the growth rate γ_{max}/ω_{ce}, optimized with respect to ka_b/ω_{ce}, and its corresponding wave frequency ω_{max}/ω_{ce} are plotted as functions of Θ. Figure 8 indicates that ω_{max} and γ_{max} decrease with Θ. As Θ approaches 90°, the wave frequency decreases to the lower hybrid frequency.

The characteristics of the wave frequency shown in Figure 6

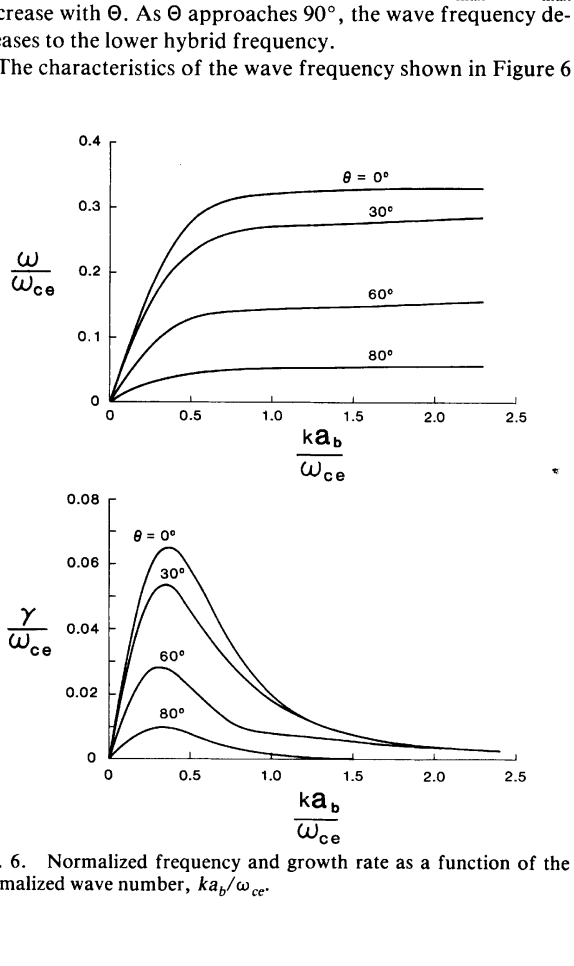

Fig. 6. Normalized frequency and growth rate as a function of the normalized wave number, ka_b/ω_{ce}.

can be qualitatively understood if one uses $\omega/k_{||}a_h << 1$ and $(\omega - k_{||}a_b)/k_{||}a_b << 1$ to approximate D_h and D_b. The real part of (3) can then be solved to yield

$$\omega^2 = [B - \sqrt{(B^2 - 4AC)}]/(2A) \qquad (4)$$

where

$$A = 1 + (1 - q)(1 - r)\frac{2\omega_{pe}^2}{k^2 a_h^2} + (1 - q)\, r\, \frac{2\omega_{pe}^2}{k^2 a_b^2}$$

$$B = A\,\omega_{ce}^2 + \omega_{pi}^2 + q\,\omega_{pe}^2$$

$$C = (\omega_{pi}^2 + q\,\omega_{pe}^2 \cos^2\Theta)\,\omega_{ce}^2$$

For small ka_b/ω_{ce}, it can be easily shown from (4) that ω is linearly proportional to ka_b. For large ka_b/ω_{ce}, it is found that ω approaches the resonance frequency of the whistler mode, $\sqrt{q}\,\omega_{pe}\cos\Theta$. When the cold electron density is a small percentage of the total density (small q), the upper frequency cutoff of the electrostatic whistler would be much smaller than f_{pe}.

When only the $n = 0$ harmonic is kept in the calculation of D_h and D_b in (3), the growth rate is reduced merely by 10% for $ka_b/\omega_{ce} < 0.5$. This result agrees with the findings of *Lotko and Maggs* [1981] that cyclotron resonance by auroral electron beams is not important for the excitation of electrostatic waves at frequencies below ω_{pe}. The wave amplification is thus mainly due to Landau resonance. Since $n = 0$ harmonic terms are dominant in the dispersion equation, the wave instability can be considered as Cherenkov-Cherenkov interactions between electron beams and the ambient cold plasma [*Mikhailovskii*, 1974]. The hot isotropic plasma plays the role of reducing the growth rate by Landau damping. The wave amplification of cusp hiss is thus similar to the Cherenkov amplification of auroral hiss in the nightside auroral zone. One difference is that auroral hiss in the nightside is believed to be excited at large wave normal angles by energetic keV electron beams [*Maggs*, 1976, 1978]. Because the cusp upward electron beams have much lower energies (<100 eV) and higher densities, they can excite more easily whistler waves near a small resonance cone.

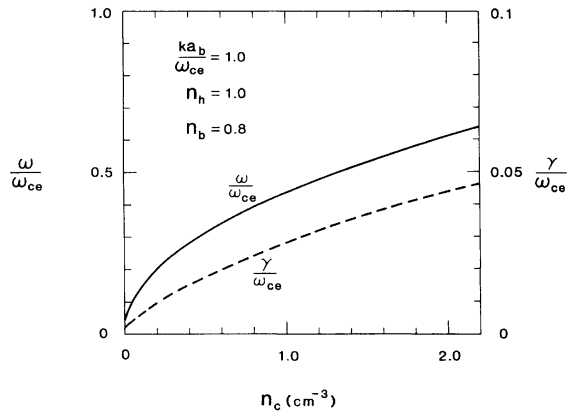

Fig. 7. Normalized frequency and growth rate as a functin of cold plasma density for constant ka_b/ω_{ce}, n_h and n_b.

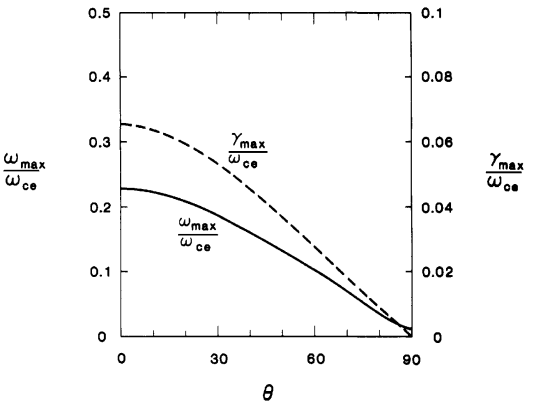

Fig. 8. Maximum of normalized growth rate with respect to the normalized wave number and its corresponding frequency as a function of the angle Θ between the wave vector and the magnetic field direction.

CUSP HISS PROPAGATION AND SOURCE

The funnel-shaped appearance of the auroral hiss spectrum has been interpreted as due to a propagation effect of whistler waves from a spatially localized source. The funnel shape of the cusp hiss spectrum shown in Plate 3 can be interpreted in the same way. We follow the approach taken by *Gurnett et al.* [1983] in estimating the low altitude boundary of the wave source from the funnel shape of the cusp hiss spectrum. We describe briefly the analysis below.

For whistler waves, propagating with a wave normal angle near the resonance cone, the ray path direction is at an angle ψ with respect to the magnetic field. The angle ψ can be written as [Stix, 1962]

$$\tan^2\psi = [f^2(1 + f_{pe}^2/f_{ce}^2) - f_{pi}^2]/(f_{pe}^2 + f_{ce}^2 - f^2) \qquad (5)$$

where f_{pi} is the ion plasma frequency. Because the approximation $f < f_{pe} < f_{ce}$ is used in the derivation, (5) is suitable for ray tracing in the low-density region. Equation (5) indicates that Φ approaches 90° as the frequency increases from the lower hybrid resonance frequency to f_{pe}. Since f_{pe} decreases with increasing altitude, the ray path of an upward propagating wave starts out along the magnetic field and then deviates to a larger angle from the magnetic field as f approaches the local f_{pe}. By tracing the shape of the low-frequency cutoff, the low altitude boundary of the source is then determined.

To compute f_{pe} along the ray path we use a plasma density n, which varies as $R^{-3.85}$ (R is the radial distance). This density model has been obtained empirically by *Persoon et al.* [1983] by using the DE-1 determination of the electron plasma frequency in the polar cap region between 2.0 and 4.7 R_E. As suggested by the upper frequency cutoff of cusp hiss in Plate 3 and Figure 4, n is assumed to be about 2.5 cm^{-3} at the DE-1 altitude equatorward of the polar cusp. We therefore use a density model $n = 2.5\ (4/R)^{3.85}$ for ray tracing. The plasma thermal effect is neglected in the computation of the ray path direction by using (5). The dipole field model is adopted for the magnetic field. A series of ray tracing fits to the funnel shape detected during the pass of day 81279 for various source positions are shown in Figure 9. The best fit is obtained when the low altitude boundary of the source is at about 1.1 R_E and the low-latitude boundary of the source is about 73°. Since

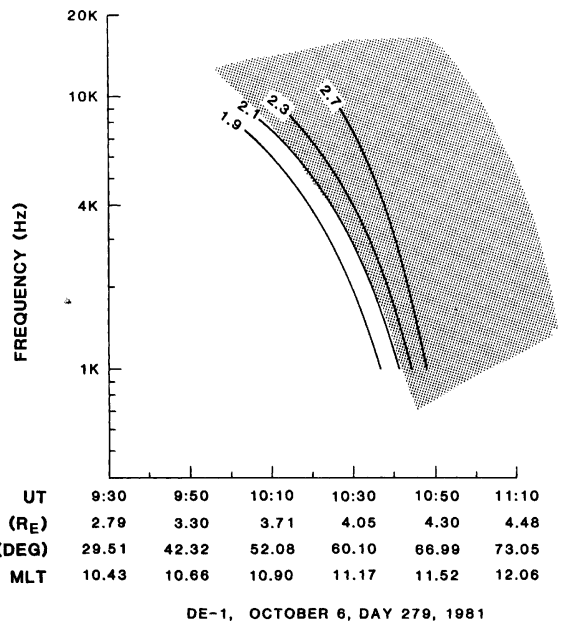

Fig. 9. Frequency-time boundaries computed from ray paths of electrostatic whistler-waves for a range of source radial distances. The shaded area corresponds to the funnel-shaped cusp hiss emission in Plate 3.

only half a funnel is detected on this pass, the high-latitude boundary of the source could not be estimated by this method.

SUMMARY AND DISCUSSION

With the DE-1 plasma and wave measurements we have demonstrated the correlation of low-energy electron beams with auroral hiss emission at a few kHz at altitudes above 2 R_E near the polar cusp. The cusp auroral hiss was interpreted as upward propagating electrostatic whistler waves at frequencies below the electron plasma frequency. The electron beams were observed streaming in both upward and downward directions with beam energies below 100 eV. The upward beams were generally more intense than the downward beams by one order of magnitude in number density.

From the comparison of the funnel shape of the cusp hiss spectrum with the ray tracing of whistler wave mode propagating near the resonance cone, we infer the low-altitude boundary of the wave source to be near 7000 km and the low-atitude boundary of the wave source to be near 73°. Since electron beams detected at about 2 R_E directly above the wave source were still intense, the wave source should be extended along the field line. Our estimate of the low-altitude boundary of the wave source agrees well with the electron acceleration region deduced by *Burch et al* [1983] for the same event. They estimated the electron acceleration region from the electron velocity distribution function and concluded that these electron beams were accelerated near 1 R_E. The slight difference in these two estimates can be easily attributed to uncertainties in the density model used in the ray tracing and the neglect of spacecraft potential when determining the potential drop.

An instability analysis has been conducted by using the plasma parameters determined during the detection of intense upward electron beams. The computed frequency of unstable electrostatic waves is found to be in good agreement with the observed frequency of cusp hiss.

The wave spatial growth length s can be estimated by using the definition $s = V_g/\gamma$. We compute V_g by taking $d\omega/dk$ and found V_g is about 0.5 a_b when $\Theta = 30°$ and $\omega/\omega_{ce} = 0.1$. The group velocity V_g decreases to zero monotonically with frequency. Using the growth rate given in Figure 6, we estimate that the spatial growth length is about 0.5 km for $\omega/\omega_{ce} = 0.1$ and decreases to about 0.1 km as ω/ω_{ce} increases to 0.2. This range of spatial growth lengths agrees with the estimate by *James* [1976]. The path length for wave growth by e^{10} is therefore only a few kilometers much less than the typical scale length of auroral structures at DE-1 altitudes. The growth rates computed are thus sufficiently large to explain the production of electrostatic whistler waves.

Because of Landau damping by the hot plasma, the growth rate shown in Figure 6 is smaller than the maximum growth rate predicted by two-stream instability in the absence of hot plasma. Without the hot background plasma, the maximum growth rate for two-stream instability γ_{max} is $\sqrt{3}\,(1-q)^{1/3}\,q^{1/6}\,\omega_{pe}\cos\Theta/2^{4/3}$ [*Mikhailovskii*, 1974]. For the parameters used in this study, γ_{max}/ω_{ce} of two-stream instability is roughly 0.34 $\cos\Theta$, about one order magnitude larger than the maximum growth rate shown in Figure 8.

Since the instability is found to be mainly due to Landau resonance, the waves are amplified through the Cherenkov-Cherenkov interaction between the electron beam and the ambient plasma. The upward propagating cusp hiss is therefore excited in the same manner as the downward propagating auroral hiss, with the exception that the responsible electron beams are in opposite directions and have different energies.

Acknowledgements. We wish to thank J. D. Menietti and C. S. Wu for useful discussions on this paper and Richard Huff for his assistance in data analysis. The work at Southwest Research Institute was supported by NASA contract no. NAS5-25693, AFGL contract F19628-82-K-0024, and Southwest Research Institute internal research project 15-9296. The work at the University of Iowa was supported by NASA/GSFC contract NAS5-25690, NASA grant NGL-16-001-043, and by the Office of Naval Research.

The Editor thanks R. Benson and another referee for their assistance in evaluating this paper.

REFERENCES

Berchem, J., and C. T. Russell, The thickness of the magnetopause current layer: ISEE 1 and 2 observations, *J. Geophys. Res., 87*, 2108, 1982.

Burch, J. L., Effects of the interplanetary magnetic field on the auroral oval and plasmapause, *Space Sci. Rev., 23*, 449, 1979.

Burch, J. L., J. D. Winningham, V. A. Blevins, N. Eaker, W. C. Gibson, and R. A. Hoffman, High-altitude plasma instrument for Dynamics Explorer-A, *Space Sci. Instrum., 5*, 455, 1981.

Burch, J. L., P. H. Reiff, R. A. Heelis, J. D. Winningham, W. B. Hanson, and J. N. Barfield, Plasma injection and transport in the mid-altitude polar cusp, Geophys. Res. Lett., 9, 921, 1982.

Burch, J. L., P. H. Reiff, and M. Sugiura, Upward electron beams measured by DE-1: A primary source of dayside region 1 Birkeland currents, *Geophys. Res. Lett., 10*, 753, 1983.

Gurnett, D. A., A satellite study of VLF hiss, *J. Geophys. Res., 71*, 5599, 1966.

Gurnett, D. A., and L. A. Frank, VLF hiss and related plasma observations in the polar magnetosphere, *J. Geophys. Res., 77*, 172, 1972.

Gurnett, D. A., S. D. Shawhan, and R. R. Shaw, Auroral hiss, Z mode radiation and auroral kilometric radiation in the polar magnetosphere: DE-1 observations, *J. Geophys. Res., 88*, 329, 1983.

Hasegawa, A., *Plasma Instabilities and Nonlinear Effects*, Springer-Verlag, Heidelberg, 1975.

Hoffman, R. A., and T. Laaspere, Comparison of very-low-frequency auroral hiss with precipitating electrons by the use of simultaneous data from two Ogo 4 experiments, *J. Geophys Res., 77*, 640, 1972.

Hoffman, R. A., and E. R. Schmerling, Dynamics Explorer program: An overview, *Space Sci. Instrum., 5*, 345, 1981.

James, H. G., VLF saucers, *J. Geophys. Res., 81*, 501, 1976.

Lin, C. S., and R. A. Hoffman, Observations of inverted-V electron precipitation, *Space Sci. Rev., 33*, 415, 1982.

Lotko, W., and J. E. Maggs, Amplification of electrostatic noise in cyclotron resonance with an adiabatic auroral beam, *J. Geophys. Res., 86*, 3449, 1981.

Maggs, J. E., Coherent generation of VLF hiss, *J. Geophys. Res., 81*, 1707, 1976.

Maggs, J. E., Electrostatic noise generated by the auroral electron beam, *J. Geophys. Res., 83*, 3173, 1978.

Meng, C.-I., Case studies of the storm time variation of the polar cusp, *J. Geophys. Res., 88*, 137, 1983.

Mikhailovskii, A. B., *Theory of Plasma Instabilities*, p. 135, Consultants Bureau, New York, 1974.

Parks, G. K., K. A. Anderson, C. Gurgiolo, C. S. Lin, R. P. Lin, F. Martel, and H. Rome, Dual spacecraft observations of energetic particles in the vicinity of the magnetopause, bow shock, and the interplanetary medium, *Space Sci. Rev. 22*, 765, 1978.

Persoon, A. M., D. A. Gurnett, and S. D. Shawhan, Polar cap electron densities from DE-1 plasma wave observations, *J. Geophys. Res., 88*, in press, 1983.

Shafranov, V. D., Electromagnetic waves in a plasma, *Rev. Plasma Phys., 3*, 1, 1967.

Sharp, R. D., R. G. Johnson, and E. G. Shelley, Observation of an ionospheric acceleration mechanism producing energetic (keV) ions primarily normal to the geomagnetic field direction, *J. Geophys. Res., 82*, 3324, 1977.

Shawhan, S. D., Magnetospheric plasma wave research *1975-1978, Rev. Geophys. Space Phys., 17*, 705, 1979.

Shawhan, S. D., D. A. Gurnett, D. L. Odem, R. A. Helliwell, and C. G. Park, The plasma wave and quasi-static electric field instrument (PWI) for Dynamics Explorer-A, *Space Sci. Instrum., 5*, 535, 1981.

Stix, T. H., *The Theory of Plasma Waves*, p. 14, McGraw-Hill, New York, 1962.

Swift, D. W., and J. R. Kan, A theory of auroral hiss and implications on the origin of auroral electrons, *J. Geophys. Res., 80*, 985, 1975.

J. L. Burch and C. S. Lin, Department of Space Sciences, Southwest Research Institute, P.O. Drawer 28510, 6220 Culebra Road, San Antonio, TX 78284.

D. A. Gurnett and S. D. Shawhan, Department of Physics and Astronomy, University of Iowa, Iowa City, IA 52242.

**(Received May 11, 1983;
revised August 8, 1983;
accepted September 23, 1983.)**